

Finite Element Analysis and Experimental Study on the Thermal Resistance Characteristics of Motor Coolers

Ke Xu ^{*}, Jie Yang ^{†‡}, Chuansheng Tang [§], Qiang Zhao [¶], Tao Li ^{||}

Abstract

Motor coolers are operated with the coupling of temperature and pressure fields, in which the change rule is affected by multiple factors. In this study, the thermal resistance of the motor cooler was examined using the velocity coefficient method to reveal the influence of heat transfer and wind resistance. The temperature and pressure fields were analyzed using the finite element method based on the hydrodynamics and momentum theorem. By varying the heat transfer and wind resistance coefficients to reflect temperature and pressure characteristics, wind and water velocities were determined. Results demonstrate that the total convective heat transfer and wind resistance coefficients of the cooler model are sensitive to variations in face-to-face wind velocity, but not to those of the cooling water flow rate. When wind velocity increases from 0.8 to 5.19 m/s, the total convective heat transfer increases by 1.85 times and wind resistance increases by 18.74 times. Variations in cooling water velocity has little effect on the Nusselt number on the air side and the Euler number of the single row tube, which are multiplied with the increase of the Reynolds number. When the Reynolds number increases from 1020 to 6345, the Nusselt number increases by 2.05 times and the Euler number decreases by 2.29 times. The results provide references for the design and performance testing of high-power motor coolers.

Keywords: cooler, thermal resistance characteristics, finite element analysis, heat transfer coefficient, drag coefficient, velocity coefficient

1 Introduction

The motor cooler is a heat exchange device that cools fluids, commonly using water, air, or oil as a coolant to

remove heat. The cooler is an indispensable device for large electrical equipment such as high-power silicon rectifiers, induction furnaces, generators and motors. The thermal medium of the tubular cooler starts from the nozzle inlet on the cylinder and flows to the nozzle outlet in sequence through baffle channels. The thermal medium adopts a double tube flow: from the water inlet through the water distribution cover, the flow enters half of the cooler pipe and then moves into the other half from a return cover to the other side and water outlet pipe. The double pipe pass flow of cold medium discharges the residual heat of the absorbing hot medium from the outlet to maintain the rated working temperature. This two-way (even four-way) flow mode intensifies the cooling effect and is thus widely used in shipbuilding, large turbo-generators, ground heating, metallurgy, and other industries [1]; [2]; [3]; [4].

However, the increasing generator power and capacity requires increasing capacity from the design technology of motor coolers. The design is a complex coupling of temperature, velocity, and pressure fields. The fin structure, type of cooling medium and cooler velocity affects the system performance, especially the running velocity of the cooling medium.

On this basis, previous studies have examined the factors affecting the heat transfer and resistance coefficients of cooler design [5]; [6]; [7]; [8], including the thermal characteristics of a turbine oil cooler [5], heat exchange and stability of an aeroengine microchannel cooler [6], and thermal characteristics of an indirect evaporative cooler etc. In recent years, theoretical, experimental and computational fluid dynamics (CFD) methods have been used to design flat fin heat exchangers [7]. However, the influence of wind and water velocities on the heat transfer and resistance are rarely explored, which restricts the application of coolers in large motors. Therefore, it is exceedingly important to accurately predict the thermal resistance characteristics and define their change rule in actual operation.

In this study, a model of the motor cooler was constructed using the finite element method to analyze the temperature and pressure fields under varying

^{*}Henan Institute of Technology, Henan Province, 453000, China [e-mail](#)

[†]Corresponding author, Henan Institute of Technology, Henan Province, 453000, China [e-mail](#)

[‡]Henan Key Equipment Engineering Research Center for New Energy Power Generation, Henan Province, 453000, China [e-mail](#)

[§]Nanyang Institute of Technology, Henan Province, 473004, China [e-mail](#)

[¶]Wolong Electric Nanyang explosion proof Group Co., Ltd, Nanyang Henan 473004, China [e-mail](#)

^{||}Department of Informatics, University of Zurich, Zurich, 8050, Switzerland [e-mail](#)

wind and water velocities. Experiments are carried out to clarify the change rule in terms of the heat transfer and resistance coefficients and the meshing relationship between the side Nusselt number reflecting the thermal resistance characteristics and the Euler number with the Reynolds number. Thus, the model improves prediction accuracy for thermal resistance performance, which can provide a reference for the development and optimization of large capacity motor coolers.

2 State of the art

Extant studies on mechanical and electrical system coolers focus on the cooling medium, cooling pipe form and other parts. Meng et al. [9] adopted numerical simulation to determine the influence of the number of cooling pipes on the flow and temperature of the air-cooled cooler of an asynchronous motor. Considering reed winding bearing of the fault prone vertical motor, Shu et al. [10] studied the thermal resistance of the cooler with varying numbers of arc plates and cooling pipes. The thermal coupling between the SLC in the array had an adverse effect on cooler performance. Sahu et al. [11] studied the effects of coupling characteristics between the superlattice coolers, geometric parameters (such as separation of the superlattice structure and the grounding electrode), convective heat transfer coefficient, and activation current on SLC using an electrothermal model. The study placed considerable importance on the optimal design of a thermal management hybrid microfluidic SLC cooling scheme with multiple cluster hotspots in microprocessors. With the miniaturization of devices and increasing power of packaging, high performance thermal management solutions for MOSFET and other power electronic devices have constantly been in demand. Walsh et al. [12] developed a micro injector and embedded this into the substrate of heating equipment, eliminating several layers of thermal resistance that were common in advanced packaging and thereby improving the dissipation efficiency without studying the heat transfer mechanism. Given that equipment was undergoing continuous miniaturization, low-cost embedded micro jet cooling technology played an important role in the design of advanced high-power density electronic products. Ouyang et al. [13] experimented on the heat transfer characteristics of oil-cooled coolers in steam turbine generators, and obtained the relationship between the heat transfer coefficient and variations of oil temperature and velocity. However, the change rule of the resistance coefficient was ignored. In attempting a systematic cooler design, Liu et al. [14] examined the water supply form, material,

and structure of the electric oil cooler. The study provided a heat loss analysis and calculation for motor thrust bearing, and proposed the design method and theoretical calculation basis for the cooler design. Santosa et al. [15] studied the overall heat transfer coefficient of two CO₂ gas coolers using experiments and computational fluid dynamics (CFD), which provided accurate prediction of the overall heat transfer coefficient. Results demonstrated that optimizing the circuit design improved the gas cooler performance by up to 20%. Carbon dioxide (CO₂) was the main refrigerant of the gas cooler in the vapor compression refrigeration system. To determine the local heat transfer rate change in the coil, Santosa et al. [16] used the CFD model to study the local refrigerant and air heat transfer coefficient in the coil of a general finned tube gas cooler. However, the change rule and influencing factors of wind resistance were largely ignored. To adapt to the challenges in the design of a transcritical CO₂ refrigeration system in a typical environment, Gupta et al. [17] established a mathematical model of an air-cooled finned tube gas cooler in a complex environment, and carried out experimental verification and engineering application. However, the proposed model was difficult to apply in idle, narrow, and closed motor systems. Based on CFD, an analysis model of an automobile cooler unit was created. Zheng et al. [18] simulated and analyzed the velocity field, temperature, and pressure fields of the cooler, and focused on the influence on cooling performance of: fin thickness, fin spacing, fin gap, fin width, fin length, and other parameters. However, no analysis was made on the influence of medium velocity on system performance. Mu et al. [19] used the gas thermal coupling method to analyze the thermal strain characteristics of high-pressure turbine guide vanes with two cooling structures, and put forward a structural optimization design scheme. The thermal deformation caused by the structural change was examined, but the capability transformation in the heat transfer was neglected. To effectively improve the large flow resistance of the tank and tube cooler, Yuan et al. [20] used numerical simulation and experimentation to analyze the influence of the cooler structure on the flow and heat transfer and proposed a new improvement scheme. However, the flow medium was not studied. Arslan et al. [21] studied the influence and design of air and water cooling on photovoltaic collectors. Saglam et al. [22] studied the thermal resistance characteristics of olive oil extraction through experiments. Hoseini et al. [23]; [24]; [25] carried out numerical simulation and experimental studies on the heat transfer characteristics of different types of coolers. Increasing the gas flow rate resulted in almost constant heat transfer efficiency of the chimney cooler, which was significantly higher than that of the

shell tube cooler and Nusselt number. However, the law of cooler pressure change lacked similar examination.

The above analyses mainly examined the heat transfer characteristics of the cooler based on structure size and single medium type, but the thermal resistance characteristics of the cooler were largely ignored. Thus, the present study adopts CFD to establish the temperature calculation model of the cooler, analyze the temperature, velocity and pressure fields, and build the cooling test system. Through the experimental data analysis, the change rule of the heat exchange and wind resistance coefficients of the cooler is obtained and used as basis for the engineering design of large-scale motor coolers.

The remainder of this study is organized as follows. Section 3 describes the cooler structure and builds its temperature calculation model and the experimental system. Section 4 uses the experimental data to analyze the cooler temperature and pressure through the finite element method of CFD and the heat transfer characteristics. Numerical simulation and experimental study show that the variation laws of the heat transfer and wind resistance coefficients can be obtained using the wind and water velocities. In addition, the variation laws of the Nusselt number on the air side and the Euler number on the single row tube is determined with the Reynolds number and wind velocity. Section 5 summarizes the conclusions.

3 Methodology

3.1 Cooler model

3.1.1 Physical model

The air face of the cooler is 638.4mm high and 500mm wide, and the length along the air flow is 110mm, as shown in Figure 1. Along the air flow direction, three rows of cooling pipes (19, 18, 19) are staggered and horizontally arranged. Each cooling pipe has an effective heat exchange length of 500mm, specification of $13.6 \times \text{mm}$, and material made of BFe30-1-1. The fins are arranged vertically and connected with the cooling pipe by the expanding process. The fins are made of copper T2 with a thickness of 0.17mm. The cooling water in the pipe undergoes a U-shaped process, that is, water flows in the lower half of the pipe and flows out of the upper half of the pipe. Figure 2 shows the structure of the cooler fins.

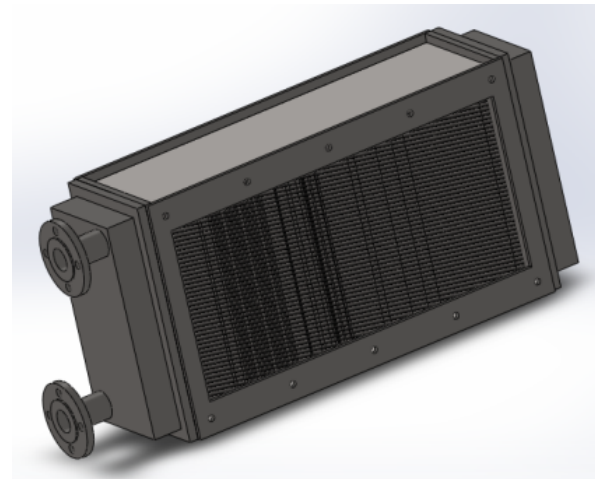


Figure 1: Outline drawing of cooler fins

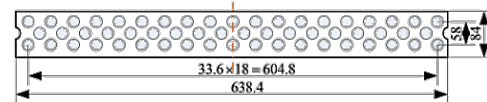


Figure 2: Structure of cooler fins

3.1.2 Establishment of calculation model

The cooler is divided into three dimensions by Solidwork, as shown in Figure 3. External air flows from the air inlet to the air outlet and forms the air-cooling circulation system. The water medium enters the upper water tank through the cooling pipe from the water inlet, and then flows out from the lower water tank through the water outlet to form the water-cooling circulation system. These two systems are separated by the water tank partition plate.

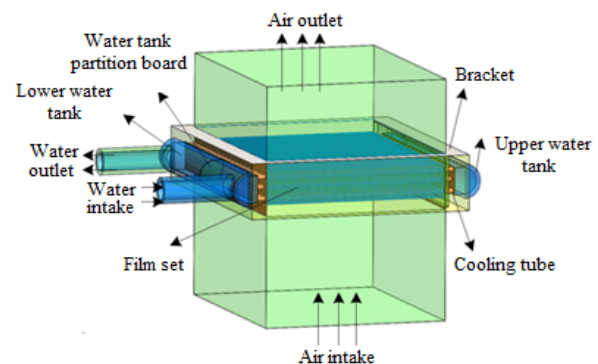


Figure 3: Cooler calculation model

To ensure the accuracy of the CFD calculation grid, the division is carried out using polyhedron grid tech-

nology and the total number of calculation grid is 5.5 million, as follows: air part grid is 4.109 million, water part grid is 813000, pipe part grid is 365000, and the water tank part grid is 213000. The polyhedron grid technology meets the calculation accuracy requirements. Figure 4 shows the structure of the cooler grid.

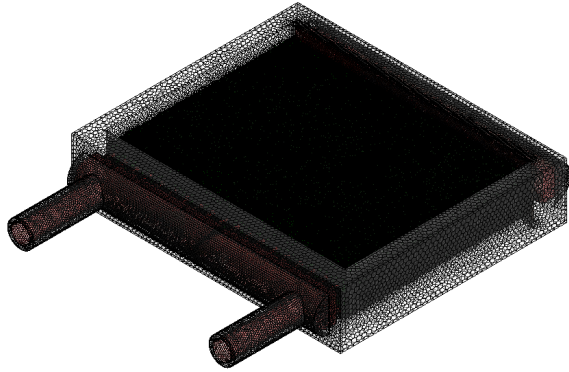


Figure 4: Cooler grid structure

3.1.3 Calculation method and boundary conditions

The Reynolds time average method is used to calculate the turbulent flow in the motor cooler, and the standard turbulence model $k - \epsilon$ is selected to close the control equation. In the model, the parameters are set by default, the solver is separated, the fluid inside the pipe is saturated water, and the fluid outside the pipe is dry air. The velocities at the inlet of the tube and shell sides are assumed to have uniform distribution without gravitational influence. The temperature inlet boundary condition is adopted for the air and water inlet, and pressure (atmospheric) outlet boundary condition is adopted for the outlet.

3.2 Experimental system

The experiment for the heat transfer and resistance characteristics on the fin side of the motor cooler is carried out in the high temperature circulating hot air tunnel. The test can be divided into the air and water circulation systems, as shown in Figure 5.

3.2.1 Air circulation system

In the high temperature circulating wind tunnel, air from the induced draft fan flows along the air duct to the heating section. The air is heated by the electric heater and reaches the test section along the air duct, and then the test model is scoured laterally. After the heat exchange between hot air and cooling water in the tube bundle, the hot air enters the nozzle flow

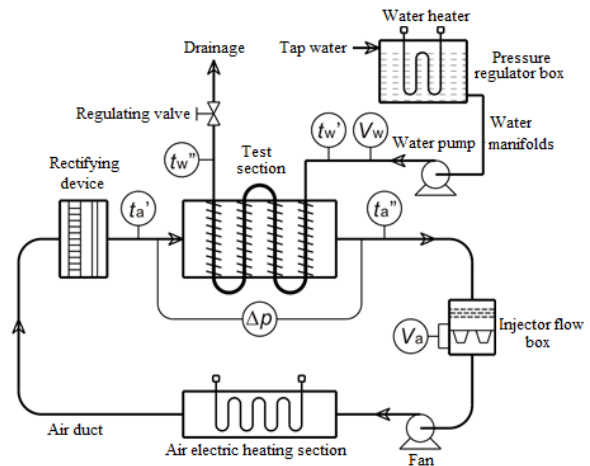


Figure 5: Test system for heat exchange and resistance characteristics of motor cooler (t_w' - Inlet water temperature, t_w'' - Outlet water r temperature, V_w - Water flow rate, t_a' - Inlet air temperature, t_a'' - Outlet air temperature, V_a - Air flow rate, p_a - Model air resistance)

box and finally returns to the fan to complete the circulation.

The air circulation system comprises an induced draft fan, velocity regulating motor, air electric heating section, rectifying section, steady flow section, test section (model), and air flow measurement section (nozzle flow box). The air duct is covered with a glass fiber insulation layer.

(1) Fan and motor: The system uses a Y9-35-1 (No.8) centrifugal fan and a JZS2-8-2 three-phase alternating current commutator motor. Table 1 shows the main parameters of the fan and motor. During the test, air volume can be adjusted using the motor velocity to meet the requirements of different test conditions.

(2) Electric heater: Air is heated in the test using an electric heater with total power of 135kW. To facilitate regulation and control, the power is divided into four groups: 54kW, 27kW, 13.5kW and 0-13.5kW. The power of the last group is adjustable and all four groups cooperate to provide stepless regulation in the power range.

(3) Rectifying device: The test requires a stable and uniform air flow into the model. A deflector is installed in the curve before the test section to reduce deflection and direct the air flow, and a rectifying net is installed behind the curve section to cut the large vortex and weaken the energy of the generated small vortex to reduce air flow turbulence. In addition, a channel with the same cross section as that of the test section is placed in front, where a current stabi-

Table 1: Main parameters of fan and motor of test system

		Fan parameters		Motor parameters	
Velocity (rpm)	Total pressure (mmH ₂ O)	Maximum air volume (m ³ /h)	Medium temperature (°C)	Velocity (rpm)	Power (kW)
1450	220	24160	<200	160-1600	4-40

lizer composed of a rectangular grid is arranged.

(4) Test section: The tube bundle (model) with a length of 150kW is placed in the test section.

(5) Nozzle flow box: The nozzle flow box is employed to measure the air flow, and four nozzles with different diameters are installed inside. A reasonable nozzle combination can be selected for measurement, adapted to the air volume under different test conditions to improve measurement accuracy.

3.2.2 Water circulation system

The water circulation system includes a stabilized pressure water tank, water heater, water pump, regulating valve, electromagnetic flow meter and test tube bundle. The stabilized pressure water tank is equipped with an electric heater with total power of 48kW. The electric heater is divided into three groups of 24kW, 12kW and 0-12kW, which can provide stepless regulation of water temperature. The feed water enters the test tube bundle to cool the hot air and then partially flows out into the sewer.

3.2.3 Test data acquisition system

The test data acquisition system comprises hardware and software. The hardware system of data acquisition mainly includes a computer, two ADAM-4118 modules, and one ADAM-4520 module. The millivolt level potential signal output by the thermocouple is collected through the voltage port of the ADAM-4118 module and is converted into digital signal input computer through the ADAM-4520 module. The 4-20mA standard current signal output of the electromagnetic flowmeter, differential pressure transmitter, and pressure transmitter is collected through the current port of the ADAM-4118 module and is converted into digital signal input computer through the ADAM-4520 module. To provide real-time detection and on-line collection of the main test parameters, the data acquisition software system stores the test data in real time and displays them dynamically.

3.3 Data processing

3.3.1 Heat transfer coefficient

The air heat release Q_a is calculated as follow:

$$Q_a = Cp_a m_a (t''_a - t'_a)$$

where m_a is the mass air flow, kg/s. t'_a is the inlet air temperature of the test piece, t''_a is the outlet air temperature of the test piece, and Cp_a is the average specific heat of air at constant pressure.

The water absorption heat Q_w is calculated as follows:

$$Q_w = Cp_w m_w (t''_w - t'_w)$$

where m_w is the water mass flow, kg/s. t'_w is the inlet air temperature of the test piece, t''_w is the outlet air temperature of the test piece, and Cp_w is the specific heat of horizontal uniform pressure, and kJ/(kg·°C).

During the test, when the relative error of air side heat release Q_a and water side heat absorption Q_w is less than ±3%, then the working condition is considered to reach stability. Thus, the total heat exchange Q assumes the value of the air heat release Q_a , that is, $Q = Q_a$.

According to the principle of heat transfer, the heat transfer coefficient K based on the entire wing side heat transfer is

$$K = \frac{Q_a}{A_o \cdot \nabla t_m}$$

where K is the heat transfer coefficient based on total area of wing side heat transfer, W/(m²·°C). A_o is the total heat transfer area on the fin side of the tube bundle, that is, $A_o = A_f + A_t$. A_f is the fin surface area, A_t is the smooth part outside the finned tube, and m^2 . ∇t_m is the logarithmic average temperature and pressure, °C. The following expression can be calculated using the counter current arrangement,

$$\nabla t_m = \frac{(t'_a - t''_w) - (t''_a - t'_w)}{\ln \frac{t'_a - t'_w}{t''_a - t''_w}}$$

3.3.2 Determining the side convection heat transfer coefficient

Analysis of heat transfer of the finned tube shows that:

$$\frac{1}{K} = \frac{A_o}{a_o(A_t + \eta_f A_f)} + \frac{\delta_t}{\lambda_t} \cdot \frac{A_o}{A_m} + \frac{1}{\alpha_i} \cdot \frac{A_o}{A_i}$$

Therefore, the coefficient of convective heat transfer on the wing side is:

$$a_o = \left(\frac{1}{K} - \frac{\delta_t}{\lambda_t} \cdot \frac{A_o}{A_m} - \frac{1}{\alpha_i} \cdot \frac{A_o}{A_i} \right)^{-1} \cdot \frac{A_o}{(A_t + \eta_f A_f)}$$

where δ_t is the wall thickness of the base tube, m . λ_t is the thermal conductivity of the base tube, $W/(m \cdot ^\circ C)$. A_m is the heat exchange area calculated by the average diameter of the base tube, m^2 . A_i is the heat exchange area of the inner wall of the base tube, m^2 . η_f is the fin efficiency of the fin tube, assuming $\eta_f = 1.0$, and a_i is the convection heat exchange coefficient in the tube, $W/(m \cdot ^\circ C)$. In addition,

$$A_m = \frac{2\pi L \delta_t}{\ln(d_o/d_i)}$$

where L is the total length of the heat exchange tube, and $m \cdot d_o$ is the outer diameter of the base tube, and $m \cdot d_i$ is the inner diameter of the base tube, m .

The convective heat transfer coefficient α_i in the tube is calculated according to Dittus-Boelter formula, that is:

$$\alpha_i = \frac{\lambda_w}{d_i} \cdot 0.023 Re_w^{0.8} Pr_w^n$$

$$Re_w = \frac{u_w \cdot d_i}{v_w}$$

where λ_w is the thermal conductivity of water in the tube under qualitative temperature, $W/(m \cdot ^\circ C)$. Pr_w is the Prandtl number of water in the tube under qualitative temperature, Re_w is the Reynolds number of water in the tube, v_w is the kinematic viscosity of water in the tube at qualitative temperature, and m^2/s . u_w is the water velocity in the tube, m/s . The qualitative temperature is the average temperature at the inlet and outlet of the cooling water in the cooling pipe, which has the characteristic size d_i inner diameter. Air is used to heat the cooling water for this test, and thus n is taken as 0.4.

3.3.3 Determining each criterion number of the wing side

This experiment adopts dimensionless criterion numbers to characterize the heat transfer and resistance characteristics of the fin bundle wing side. With the change of Re_a , Nu_a characterizes the heat transfer of the tube bundle Eu_a , which in turn characterizes the resistance.

The Nusselt number Nu_a and Reynolds number Re_a of the wing side are respectively:

$$Nu_a = \frac{a_o \cdot d_0}{\lambda_a}$$

$$Re_a = \frac{u_a \cdot d_0}{v_a}$$

where λ_a is the thermal conductivity of air outside the pipe, $W/(m \cdot ^\circ C)$. u_a is the air flow rate between pipes, and m/s . v is the kinematic viscosity of air outside the pipe, m^2/s . The characteristic dimension d_0 is the outer diameter of the cooling pipe, and the qualitative temperature is the average air temperature at the inlet and outlet.

The Euler number Eu_a of single row tubes on the wing side is:

$$Eu_a = \frac{\nabla P_a}{N \rho_a u_a^2}$$

where ρ_a is the average density of air outside the pipe and kg/m^3 . N is the number of rows along the air flow.

Thus, the relationship between the heat transfer Nu_a and resistance characteristics Eu_a of the fin side of the cooler model with the air side Re_a can be obtained.

4 Result Analysis and Discussion

4.1 Simulation analysis

To reflect the change rule of the cooler, the finite element simulation compares and analyzes the influence of wind and water velocities on the temperature and pressure field distributions of the cooler from three working conditions. In case I, water velocity is 0.8m/s and wind velocity is 0.81m/s. In case II, water velocity is 1.0m/s and wind velocity is 0.82m/s. In case III, water velocity is 1.0m/s and wind velocity is 1.63m/s. The cloud charts of temperature and pressure fields corresponding to the three conditions are shown in Figures 6 and 7, respectively.

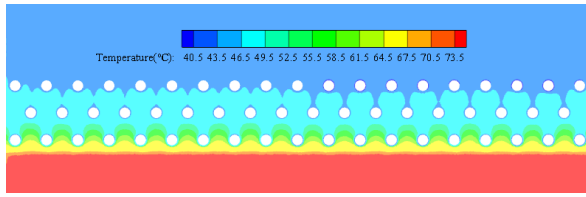


Figure 6: Water velocity 0.8m/s and wind velocity 0.81m/s

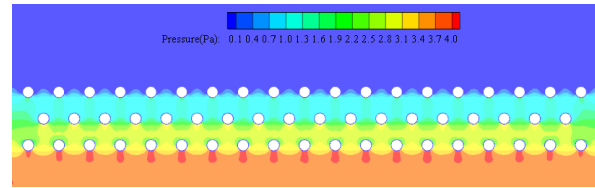


Figure 9: Water velocity 0.8m/s and wind velocity 0.81m/s

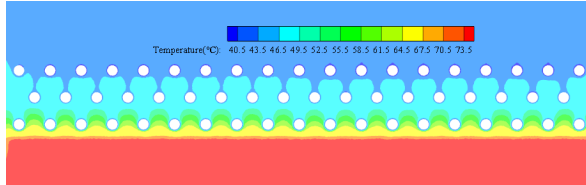


Figure 7: Water velocity 1.0m/s and wind velocity 0.82m/s

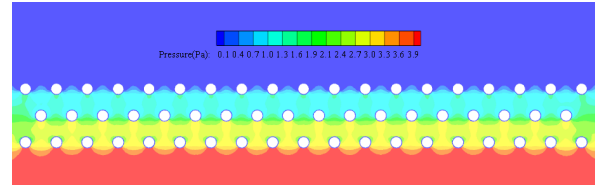


Figure 10: Water velocity 1.0m/s and wind velocity 0.82m/s

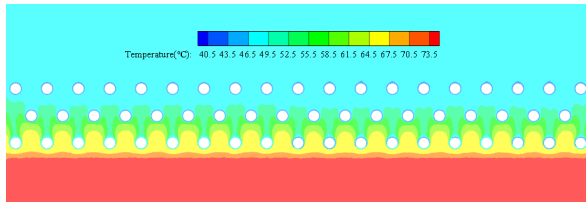


Figure 8: Water velocity 1.0m/s and wind velocity 1.63m/s

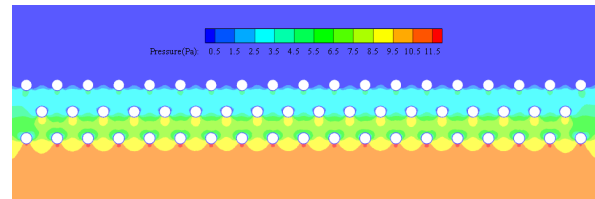


Figure 11: Water velocity 1.0m/s and wind velocity 1.63m/s (Pressure field distribution cloud chart)

The following conclusions can be drawn from Figures 6,7,8: (1) When the water velocity increases from 0.8m/s as shown in Figure 6 to 1.0m/s as shown in Figure 7 under certain wind velocity, the temperature field distribution of the cooler remains almost the same. In Figure 6, the inflow and outflow gas temperatures are 71.96 and 41.93, respectively, with a temperature difference of 33.03. In Figure 7, the inflow and outflow gas temperatures are 74.8 and 41.956, respectively, with a temperature difference of only 0.21, which is lower than when the water velocity is 1.0m/s. (2) When the water velocity is stable, the wind velocity doubles from 0.8m/s as shown in Figure 7 to 1.63m/s as shown in Figure 8. The gas discharge temperature of the cooler clearly rises, reaching 46.64. The temperature difference is only 27.43, and thus wind velocity has considerable influence on the temperature change of the cooler.

Figures 9,10,11 show the pressure field distribution of the cooler under three working conditions. The following conclusions can be drawn: (1) The pressure of the cooler decreases from the inlet to the outlet, but is redistributed when the tension increases sharply near the through-hole of the inlet side fin; (2) Fig-

ures 9 and 10 show that under certain wind velocity, the pressure field distribution of the cooler changes slightly when the water velocity increases from 0.8m/s to 1.0m/s. In Figure 9, the difference of gas pressure increases from 3.3Pa to 3.5Pa; (3) Under certain water velocity, wind velocity doubles from 0.8m/s as shown in Figure 10 to 1.63m/s as shown in Figure 11. The pressure difference of the cooler increases by 2.86 times from 3.5Pa to 10Pa. Thus, wind velocity has a considerable influence on the pressure distribution of the cooler.

4.2 Experimental analysis

The test conditions are as follows: inlet wind temperature is 75, head-on wind velocity is 0.8-5.2m/s, inlet water temperature is 40, cooling water flow rates for the three conditions are 0.8m/s, 1.0m/s, and 1.5m/s, respectively, and piece distance is 2.5mm.

4.3 Relationship of total convective heat transfer coefficient of cooler model with the cooling water flow rate and face wind velocity

Figure 12 shows the relationship of the total convective heat transfer coefficient of the three-fin tube cooler model with cooling water flow rate and face velocity. The following conclusions can be drawn: (1) At water velocity of 1.0m/s, the total convective heat transfer coefficient gradually increases with the increase of air flow rate, but the increase rate gradually declines. At wind velocity of 0.8m/s, the total convective heat transfer coefficient is approximately $35.33W/(m^2 \cdot K)$. As wind velocity increases to 5.19m/s, the total convective heat transfer coefficient increases to $65.38 W/(m^2 \cdot K)$; (2) For the same cooler, increasing the water flow rate improves the heat transfer film coefficient on the water side, and thereby, the overall heat transfer coefficient. Heat resistance mainly concentrates on the air side and the wall, and thus the change of water flow rate has little effect on the overall heat transfer coefficient of the heat exchanger. At wind velocity 0.8m/s, the total heat transfer coefficient of water velocity 0.8m/s is only $3.9 W/(m^2 \cdot K)$ higher than that at water velocity 1.5m/s.

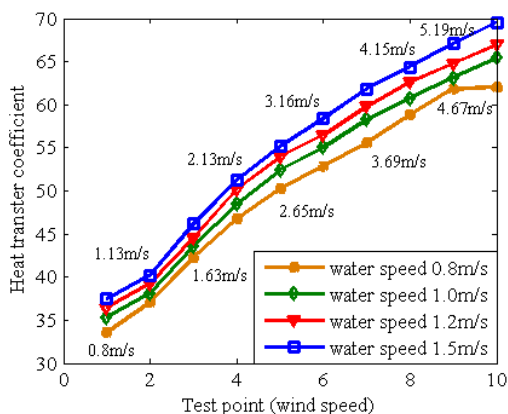


Figure 12: Relationship of heat transfer coefficient with the cooling water flow rate and face wind velocity

4.4 Relationship of wind resistance of the cooler model with the cooling water flow rate and face wind velocity

Figure 13 shows the relationship of wind resistance with the head-on wind velocity of the model and cooling water flow rate. The following conclusions can

be drawn: (1) At water velocity 1.0m/s, the wind resistance coefficient increases gradually with the increase of air velocity, and its increase rate gradually rises. At wind velocity 0.82m/s, the wind resistance coefficient is approximately 6.15Cd. At wind velocity 5.19m/s, the total convective heat transfer coefficient increases nearly 20 times to 115.26; (2) For the same cooler, the water flow velocity has a very small effect on wind resistance. At wind velocity 2.65m/s, the total heat transfer coefficient of water velocity 0.8m/s is only 0.39Cd higher than that at water velocity 1.5m/s. Thus, the heat transfer coefficient is basically unchanged.

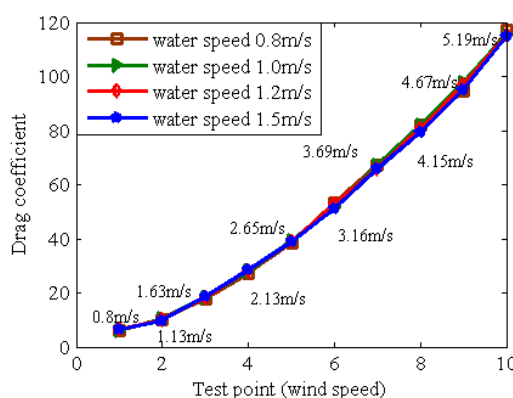


Figure 13: Relationship of wind resistance with the cooling water flow rate and face wind velocity

4.5 Relationship of Nusselt number on the air side of cooler model with the Reynolds number and cooling water flow rate at the minimum flow section

Figure 14 shows the relationship of the Nusselt number on the air side of the model with the Reynolds number and cooling water flow rate at the minimum flow section. The following conclusions can be drawn: (1) At a certain water velocity 1.0m/s, the Nusselt number on the air side gradually increases with the increase of Reynolds number, but its rate of increase gradually slows. When the Reynolds number is 1020, the Nusselt number of the air side is approximately 19.03. When the Reynolds number is 6345, the Nusselt number of the air side increases by nearly 2 times to 39; (2) For the same cooler, the effect of water flow velocity on the Nusselt number of air side is very small. When the Reynolds number is 3870, the Nusselt number of the air side at water velocity 0.8m/s is basically unchanged at water velocity 1.5m/s.

Table 2: Correlation between the air side heat exchange and resistance criteria of the cooler model

Fin spacing	Air side heat transfer correlation	Air side resistance correlation	Scope of application
2.5mm	$Nu_a = 1.2905Re_a^{0.4031}Pr^{1/3}$	$Eu_a = 20.8853Re_a^{-0.4422}$	$1000 < Re_a < 6450$

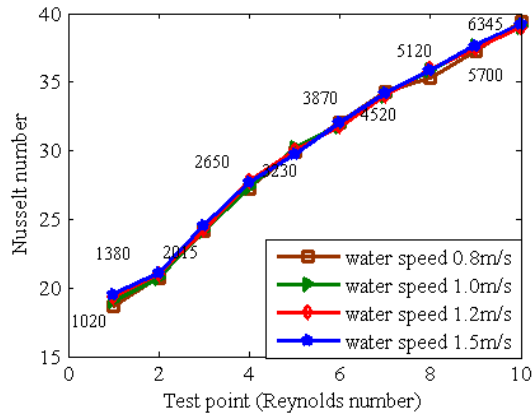


Figure 14: Relationship of Nusselt number on air side with the Reynolds number and cooling water flow rate at the minimum flow section

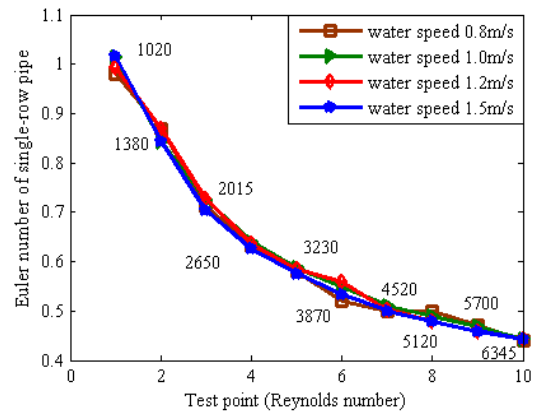


Figure 15: Relationship of the Euler number of the single row tube with the Reynolds number of the minimum flow section and the cooling water flow rate

4.6 Relationship of Euler number of single row tube of the cooler model with Reynolds number of minimum flow section and cooling water flow rate

Figure 15 shows the relationship of the Euler number of the single row tube in the cooler model with the Reynolds number and cooling water flow rate at the minimum flow section of the model. The following conclusions can be drawn: (1) At water velocity 1.0m/s, the Euler number of the single row tube gradually decreases with the increase of Reynolds number, and the decrease amplitude gradually accelerates. When the Reynolds number is 1020, the Euler number of the single row tube is approximately 1.013. When the Reynolds number is 6345, the Euler number of the single row tube decreases by nearly 2.5 times to 0.443; (2) For the same cooler, the influence of water flow velocity on the Euler number of the single row tube is very small. When the Reynolds number is 3870, the Euler number of the single row tube at water velocity 0.8m/s is 0.013 higher than that at water velocity 1.5m/s.

4.7 Correlation between the air side heat exchange and resistance criteria of the cooler model

The correlation between the air side heat transfer and resistance criteria of the cooler model can be obtained. Table 2 shows that this correlation adopts the qualitative temperature, which is the average temperature of the inlet and outlet air, and the qualitative dimension, which is the outer diameter of the cooling pipe.

4.8 Comparison of simulation results

To verify the consistency of results, Table 3 compares the data under three conditions corresponding to the simulation and experiment.

The results show that the three working conditions obtain very close temperatures at the inlet and outlet of the air circulation and water circulation channels, and the temperature difference errors at the inlet and outlet are very small. The maximum error of the air loop is 2.07% while that of the water loop is 2.5%, which confirms the validity of the simulation and experiment results.

Table 3: Comparison of simulation and experiment($^{\circ}C$)

Condition	Data item	Inlet air	Outlet air	Air	Error	Inlet	Outlet water	Water	Error
		temperature	temperature	temperature difference	(%)	temperature	temperature	Temperature difference	(%)
Water velocity 0.8m/s	Simulation	74.96	41.93	33.03	2.07	39.72	40.06	0.88	1.12
	Value								
Wind velocity 0.81m/s	Test	74.96	42.60	32.36		39.72	40.61	0.89	
	Value								
Water velocity 1.0m/s	Simulation	74.8	41.56	33.24	1.59	39.47	40.18	0.71	1.39
	Value								
Wind velocity 0.82m/s	Test	74.8	42.08	32.72		39.47	40.19	0.72	
	Value								
Water velocity 1.0m/s	Simulation	74.07	46.64	27.43	0.29	39.58	40.75	1.17	2.50
	Value								
Wind velocity 1.63m/s	Test	74.07	46.56	27.51		39.58	40.78	1.2	
	Value								

5 Conclusion

This study used a physical model and combined numerical simulation with experimental study to explore the thermal resistance characteristics of motor coolers and reveal the relationship of the heat transfer and wind resistance coefficients with the cooling medium flow rate (wind and water velocities). Thus, the influencing factors of heat transfer coefficient, wind resistance coefficient, Nusselt number of air side, and Euler number of single row tube of the cooler were analyzed. Finally, the following conclusions could be drawn:

(1) The total convective heat transfer and wind resistance coefficients of the cooler model are sensitive to variations in face wind velocity, but are largely unaffected by variations in cooling water flow rate.

(2) The Nusselt number on the air side and the Euler number of the single row tube of the cooler are multiplied with the increase of the Reynolds number, but are largely unaffected by the change of cooling water velocity.

(3) When the Reynolds number is $1000 < Re_a < 6450$, the Nusselt number on the air side and the Euler number of the single row tube can be used to quantitatively express the change relationship of the corresponding parameters.

In this study, the change rule of the thermal resistance characteristics of the cooler under the compound cooling mode is determined to provide a reference for the optimal design of the high-power motor cooler. Given that the cooler is a complex system of magnetic thermal solid coupling, this study focuses on the temperature field. Future works can use this system to

integrate the strain and magnetic change brought by temperature variations, and examines the coupling of multiple physical fields to improve the comprehensive performance and efficiency of motor coolers.

6 Acknowledgements

This study was supported by the Key Scientific Study Projects of Higher Education Institutions of Henan Province (Grant Nos. 20B470003 and 18B470007) and the Promotion Special Project of Scientific Study Program of Henan Province (Grant Nos. 202102210084 and 202102210298).

References

- Jiang, Z., Zhou, Z.J., and Jiajun, F. (2019) Design of automatic cleaning device for marine shell and tube cooler. *Journal of Zhejiang International Maritime College*, **15** (3), 74–76.
- Liu, X.L. (2009) Design of baffle plate processing and drilling die for the tube cooler of 600MW turbo-generator. *Dongfang Electrical Machine*, (5), 73–75.
- Subesh, T., Dilip, R.N., Logesh, K., Ramesh, V., Venkatasudhahar, M., and Surrya, P.D. (2020) Study on performance of horizontal single pass shell and multi-tube heat exchanger with baffles by air bubble injection. *International Journal of Ambient Energy*, **41** (6), 641–651.
- Al-Obaidi, A., and Mohammed, A. (2019) Numerical investigations of transient flow characteristic in axial flow pump and pressure fluctuation analysis based

- on the CFD technique. *Journal of Engineering Science and Technology Review*, **12** (6), 70–79.
- 5.Subramani, K., Logesh, K., Kolappan, S., and Karthik, S. (2020) Experimental investigation on heat transfer characteristics of heat exchanger with bubble fin assistance. *International Journal of Ambient Energy*, **41** (6), 617–620.
- 6.Huang, X., and Ma, X.B. (2019) The research on vibration and heat transfer characteristics of the microchannel precooler. *Energy Conservation Technology*, **37** (1), 8–12.
- 7.Librerros, N., Mercado, N., Ochoa, G., Forero, J., and Obregon, L. (2019) Critical review of the theoretical, experimental and computational fluid dynamics methods for designing plate fin heat exchanger. *Journal of Engineering Science and Technology Review*, **12** (6), 126–133.
- 8.Sun, T.Z., Huang, X., and Luo, R. (2015) Experimental study on the performance of rotary wheel indirect evaporative cooler using different secondary air. *Fluid Machinery*, **43** (5), 65–69.
- 9.Meng, D.W., Liu, H.M., Feng, S.Z., and Ji, B.Y. (2015) Design and numerical analysis for the cooler in compact high-voltage motor. *Journal of Harbin University of Science and Technology*, **20** (1), 45–49.
- 10.Shu, T., and OuYang, X.P. (2017) Experimental study on heat transfer performance of bearing oil cool with tension-wound wir-tube in the vertical motor. *Energy Research and Information*, **33** (2), 106–111.
- 11.Sahu, V., Fedorov, A.G., and Joshi, Y.K. (2014) Computational and experimental investigation of thermal coupling between superlattice coolers. *IEEE Transactions on Components, Packaging and Manufacturing Technology*, **4** (4), 622–631.
- 12.Walsh, S.M., Malouin, B.A., Browne, E., Bagnall, K., Wang, E., and Smith, J. (2019) Embedded micro-jets for thermal management of high power-density electronic devices. *IEEE Transactions on Components, Packaging and Manufacturing Technology*, **9** (2), 269–278.
- 13.OuYang, X.P., and Liu, B.X. (2016) Experimental study on heat transfer performance of finned tube turbine oil cooler. *Journal of Engineering for Thermal Energy and Power*, **31** (8), 31–37,122.
- 14.Liu, X.Q., Liu, X.Q., and Liang, Y.H. (2017) Research on the type and cooling mode of oil cylinder cooler of large and medium vertical motor. *China Rural Water and Hydropower*, (7), 196–199.
- 15.Santosa, I., Tsamos, K., Gowreesunker, B., and Tassou, S. (2019) Experimental and CFD investigation of overall heat transfer coefficient of finned tube CO₂ gas coolers. **161**, 300–308.
- 16.Santosa, I., Gowreesunker, B., Tassou, S., Tsamos, K., and Ge, Y. (2017) Investigations into air and refrigerant side heat transfer coefficients of finned-tube CO₂ gas coolers. *International Journal of Heat and Mass Transfer*, **107**, 168–180.
- 17.Gupta, D.K., and Dasgupta, M.S. (2014) Simulation and performance optimization of finned tube gas cooler for trans-critical CO₂ refrigeration system in Indian context. *International Journal of Refrigeration*, **38**, 153–167.
- 18.Zheng, D., and Zhang, R.F. (2019) Effect factors analysis of cooling performance of vehicle engine radiator system based on CFD. *Machinery Design and Manufacture*, (11), 102–106,110.
- 19.Mu, L.J., Dong, X.Z., Gao, Q., and Tan, C.Q. (2017) Effects of cooling structure on thermal Strain characteristic of high-pressure turbine guide vane. *Journal of Propulsion Technology*, **38** (7), 1610–1617.
- 20.Yuan, B., Hao, Z.Y., Li, H., and Zheng, X. (2016) Complex turbulent flow and heat transfer characteristics of spiral finned groove tubes in EGR cooler. *Journal of Zhejiang University (Engineering Science)*, **50** (8), 1507–1515.
- 21.Arslan, E., Tuncer, A., Koşan, M., Aktaş, M., and DolgunHoseini, E. (2020) Designing of a new type air-water cooled photovoltaic collector. *Tehnicki Glasnicki-Technicki Journal*, **14** (1), 41–45.
- 22.Saglam, C., Tan, F., and Aktas, T. (2018) Changing of viscosity and thermal properties of olive oil with different harvesting method and waiting period.. *Tehnicki Glasnicki-Technicki Journal*, **12** (1), 50–54.
- 23.Hoseini, S.S., Najafi, G., Ghobadian, B., Yusaf, T., and Mamat, R. (2018) Experimental and numerical analysis of flow and heat transfer characteristics of EGR cooler in diesel engine. *Applied Thermal Engineering*, **140**, 745–758.
- 24.Hoseini, S., Najafi, G., and Ghobadian, B. (2018) Thermal and fluid simulation of a new diesel engine cooling exhaust gas recirculation system to reduce exhaust gas emissions. *Journal of Advanced Research in Fluid Mechanics and Thermal Sciences*, **51** (2), 197–208.
- 25.Hoseini, S.S., Najafi, G., and Ghobadian, B. (2016) Experimental and numerical investigation of heat transfer and turbulent characteristics of a novel EGR cooler in diesel engine. *Applied Thermal Engineering*, **108**, 1344–1356.